Polymer 51 (2010) 1723–1727

Contents lists available at ScienceDirect

Polymer

journal homepage: www.elsevier.com/locate/polymer

Characterization of poly(*N*-vinyl-2-pyrrolidone)s with broad size distributions

Patrick Knappe, Ralf Bienert, Steffen Weidner, Andreas F. Thünemann*

BAM Federal Institute for Materials Research and Testing, Richard-Willstätter-Straße 11, 12489 Berlin, Germany

ARTICLE INFO

Article history:
Received 1 October 2009
Received in revised form
16 February 2010
Accepted 23 February 2010
Available online 1 March 2010

Keywords:
Small-angle X-ray scattering
SAXS
Field-flow fractionation

ABSTRACT

We report on the characterization of the solution structure of poly(*N*-vinyl-2-pyrrolidone)s (PVP) by small-angle X-ray scattering (SAXS) and by online coupling of asymmetrical flow field-flow fractionation (A4F), SAXS and dynamic light scattering (DLS). The commercial products PVP K30 and PVP K90 with nominal molar masses of 40×10^3 and 360×10^3 g mol^{-1}, respectively, were investigated separately and as binary mixture. Detailed information for all polymer fractions is available on the polymer contour lengths and the diffusion coefficients. Key areas of applications for the A4F-SAXS-DLS coupling are seen in comparison to static light scattering for polymers with radii of gyration smaller than 10 nm, for which only SAXS produces precise analytical results on the size of the polymers in solution.

© 2010 Elsevier Ltd. All rights reserved.

1. Introduction

PVP is a water-soluble versatile polymer whose application ranges from pharmaceutical and cosmetics formulations [1] to technical adhesives, coatings, inks, electronics, etc [2]. Currently PVP is found to be of increasing interest in nanotechnology especially for the protection and stabilization of metal and metal oxide nanoparticles in aqueous surroundings. For example, monodisperse silver nanocubes were synthesized in large quantities by reducing silver nitrate with ethylene glycol in the presence of PVP [3]. Furthermore, this procedure allows control over shape and size of gold nanoparticles as well [4]. PVP sterically protects nanoparticles from aggregation [5], and single-wall carbon nanotubes have been solubilized in water very successfully with PVP [6]. For cobalt it has been demonstrated that PVP interacts little with the surface of the particles and therefore would not modify their electronic and magnetic properties [7]. By contrast, the molar mass can have a strong influence on the magnetic properties of nickel nanoparticles [8]. Superparamagnetic nickel particles are formed when a PVP with medium molar mass (K30) is used for particles synthesis, but ferromagnetic particles are obtained for the high molar mass PVP (K90) [8].

The molecular characteristics of PVP were first described with great effort in the 1950s [9,10] because of its early use as blood plasma extender, for which the range of molar masses must have been adjusted. Iodine complexed PVP (povidone-iodine) has become universal for wound disinfection since it has been found to be less toxic than iodine tinctures [11]. PVP has a long-standing record in biomedical and pharmaceutical applications and currently PVP based drug delivery systems are under intense investigation [12].

In the 1990s a detailed study of the hydrodynamic properties in dilute solution was given by Pavlov et al. [13], who addressed the finding that the relationships between the intrinsic viscosity and the molecular mass vary greatly in the literature. One reason for the great differences in the reports may be that commercial PVPs display very broad molar mass distributions with ratios of M_w to M_n of typically larger than three [2]. In addition, PVP is surface active due to the presence of highly polar amide groups in conjunction with non-polar ethylene groups. This makes it attractive for complexation with low molar mass compounds or surfactants [14,15]. But the wide molar mass range in combination with its amphiphilic nature makes it very difficult to accurately characterize PVP. Nevertheless, Jones et al. were successful in developing a HPCL method for the detection of the lower molar mass PVP K15 in pharmaceutical formulations [16]. Additional attempts have been made for automated batch characterization of PVP solutions by combining SEC, static light scattering and viscometry for high molar mass PVP [17].

For technical purposes, PVP's molar masses are still classified by its K-values, which are derived from viscometry measurements [9,10]. The K-value is an integral parameter and in consequence a rough estimate of PVP's molar mass, but it is sufficient for characterization in many technical uses of PVP.

In our opinion a detailed knowledge of the PVP's solution state characteristics is necessary for a systematic development of its use in nanotechnological applications. Hence, the purpose of this work

* Corresponding author.
E-mail address: andreas.thuenemann@bam.de (A.F. Thünemann).

0032-3861/$ – see front matter © 2010 Elsevier Ltd. All rights reserved.
doi:10.1016/j.polymer.2010.02.039

is to provide a more detailed analysis on the solution structure and molecular characteristics of technically available PVPs. The present study is organized as follows. We first discuss the scattering properties of PVP with medium and high molar mass (K30 and K90, respectively) in terms of the wormlike chain model. Second, the separation of K30, K90 and a binary mixture of K30 and K90 is performed with asymmetrical flow field-flow fractionation (A4F). Third, online detection with SAXS and DLS after A4F fractionation is discussed.

2. Materials and methods

2.1. Materials

Poly(*N*-vinyl pyrrolidone)s PVP Kollidon 30 and PVP Kollidon 90 were obtained from BASF with nominal molar masses of 4.0×10^4 g mol^{-1} and 3.6×10^5 g mol^{-1}, respectively. The molecular mass of PVP is given as the K-value [18], from which the viscosity average molar mass (M_v) can be approximated. K30 corresponds to M_w and M_n values of about 5.0×10^4 g mol^{-1} and 1.5×10^4 g mol^{-1}, and K90 to 1.4×10^6 g mol^{-1} and 3.25×10^5 g mol^{-1} as measured by GPC, i.e $M_w/M_n = 3.3$ (K30) and 4.3 (K90).

2.2. Methods

2.2.1. Asymmetrical flow field-flow fractionation (A4F)

The A4F unit was purchased from Postnova Analytics GmbH (Germany), and consisted of an AF2000 focus system (PN 5200 sample injector, PN 7505 inline degasser, PN 1122 tip and focus pump) equipped with slot outlet technique for increased sensitivity [19]. The in-house built slot outlet function was implemented by using a special channel top with an additional port 13 mm in front of the laminar outlet port and by connecting a narrow capillary to the pre-installed slot outlet port of the A4F unit to control the flow by backpressure.

An inline solvent filter (100 nm, regenerated cellulose, Postnova) was placed between the solvent pumps (tip and focus) and the channel to reduce the background signals. The channel thickness was 500 μm, and the ultrafiltration membrane was a regenerated cellulose membrane with a cutoff of 5×10^3 g mol^{-1}. A solution of 0.1 M sodium chloride in deionized water with additional 200 mg L^{-1} of sodium azide to prevent bacterial growth was used as the solvent for the polymers, as well as for the carrier solution. The latter was filtered through a 0.1 μm regenerated cellulose filter, the former samples through a 0.45 μm syringe filter prior to use to avoid dust in the samples. A volume of 0.40 mL solution at a polymer concentration of 15 mg mL^{-1} was used for analysis of K30 and 0.20 mL at 5 mg mL^{-1} for K90. 0.40 mL of the K30/K90 mixture was injected with concentrations of 15 and 5 mg mL^{-1} of K30 and K90, respectively. The channel flow rate was set to 1.0 mL min^{-1} for the A4F experiment, a slot outlet function was enabled at 80% to reduce further dilution, resulting in a detector flow rate of 0.2 mL min^{-1}. The crossflow was controlled by AF2000 software from Postnova Analytics. It was set to decrease exponentially over time with an exponent of 0.25 ml min^{-2} according to the power method [20] implemented in the A4F control software, starting with a flow rate of 3 mL min^{-1} and decreasing to 0 mL min^{-1} within 60 min. For the crossflow profile see also Fig. 2. The PVP solutions were injected and focused in the separation channel within 3 min and a further 7 min interval of transition time followed before the elution started. The outlet of the A4F was connected directly to the RI detector, the flow cell of the SAXS instrument and the flow cell of the DLS device.

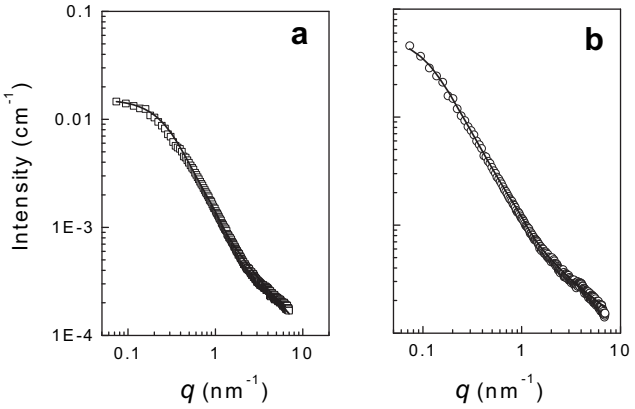

Fig. 1. Double logarithmic presentation of the SAXS curves of PVP K30 (a) and K90 (b) (symbols). Curve fits (solid lines) are from the wormlike chain model with contour lengths of 50 ± 1 nm (a) and 226 ± 6 nm (b). The Kuhn length is 3.0 nm for both.

2.2.2. Small-angle X-ray scattering (SAXS)

SAXS measurements were performed at the BAM*line* at BESSY II (Berlin, Germany) with a Kratky type instrument (SAXSess from Anton Paar, Austria) at 25 ± 1° C and with an acoustic levitator setup as described recently in detail [21,22]. The SAXSess has a low sample-to-detector distance (0.309 m), which is appropriate for investigation of dispersions with low scattering intensities. The measured intensity was corrected by subtracting the intensity of a capillary filled with pure solvent. The scattering vector is defined in terms of the scattering angle θ and the wavelength λ of the radiation (λ = 0.124 nm): thus $q = 4\pi/\lambda \sin\theta$. Deconvolution (slit length desmearing) of the SAXS curves was performed with Glatter's established indirect Fourier transformation method [23–25] implemented in the PCG Software Version 2.02.05 (University of Graz) to verify the results produced with the SAXSquant software (Anton Paar).

2.2.3. Dynamic light scattering (DLS)

The DLS measurements were performed using a particle sizer (Zetasizer Nano ZS, Malvern Instruments, UK) equipped with a He–Ne laser (λ = 632.8 nm). The scattering data were recorded at 25 ± 1 °C in backscattering modus at a scattering angle of $2\theta = 173°$, which corresponded to a scattering vector of $q = 4\pi n/\lambda \sin\theta$ (0.02638 nm^{-1}). The aqueous sample solutions were investigated in a flow through quartz cuvette.

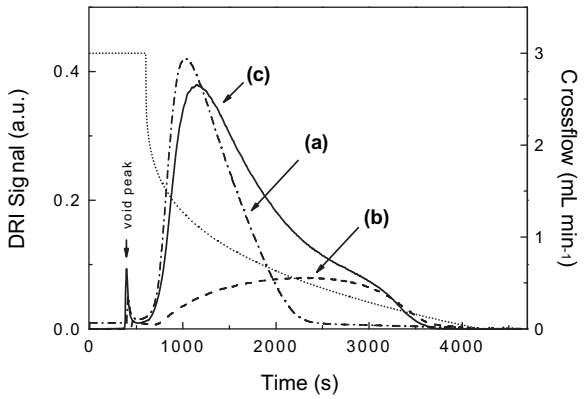

Fig. 2. Fractograms of the asymmetrical field-flow fractionation with RI detection of K30 (a), K90 (b) and a mixture of K30 and K90 (c). Right axis. Crossflow profile used for elution (dotted line).

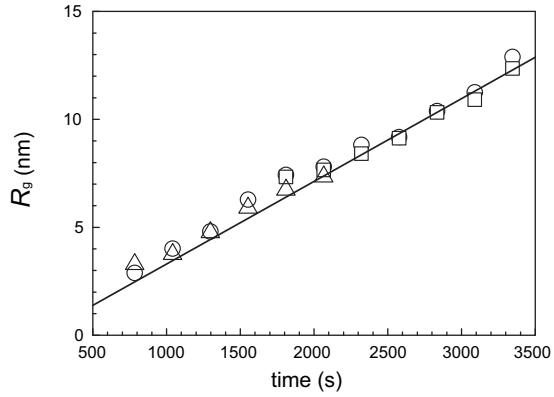

Fig. 3. The radii of gyration as a function of the fraction time for PVP K30 (triangles), K90 (squares) and mixture (circles). The linear approximation (straight line) has a slope of $(3.83 \pm 0.17)\ 10^{-3}$ nm s^{-1} and an intercept at $-(0.05 \pm 0.2)$ nm.

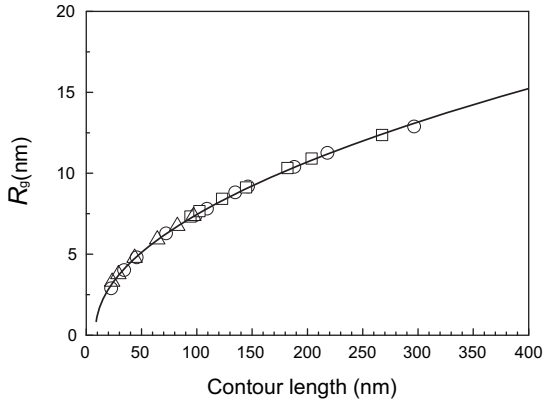

Fig. 5. The radii of gyration as a function of the contour lengths for fractionated K30 (triangles), K90 (squares) and mixture of K30 and K90 (circles). Data are listed in Table 2. The best fit of the Benoit–Doty equation corresponds to a Kuhn segment length of 3.5 nm (solid line).

3. Results and discussion

3.1. Scattering properties of PVP K30 and K90

SAXS of the non-fractionated PVPs were measured from aqueous solutions at concentrations of 0.3–1.5 % (w/w). Results for K30 and K90 are displayed in double logarithmic presentation of Fig. 1a and b, respectively (symbols). No change of the shape of the curves with concentration could be observed, and we conclude that interactions between the polymer chains can be neglected in this concentration regime. Therefore, single-chain models are appropriate for interpretation of the SAXS data; the wormlike chain model seems the most suitable for this [24].

Scattering functions for semi-flexible chains are given by Pedersen and Schurtenberger [26]. These were tested in a comparative study by Ballauff et al. to provide the best description for the scattering intensity throughout a large range of possible chain stiffnesses [27]. Small corrections of that flexible cylinder function including polydispersity of the length are provided by Chen [28] and considered in the NIST software package [29]. It calculates the form factor of a flexible chain with a circular cross section and a uniform scattering length density. The total scattering function is given as

$$I(q) = c\Delta\rho_m^2 MS(q,L,b)P(q,R) \quad (1)$$

where c is the polymer concentration, M the molar mass of the polymer, $\Delta\rho_m^2$ is the square of the electron density difference between polymer and solvent. $S(q,L,b)$ is the scattering function of a single semi-flexible chain with the contour length of the polymer chain, L, and the Kuhn length, b. The b is twice the persistence length, l_p, and a measure for the chain stiffness. The mathematical expression of $S(q,L,b)$ is lengthy and can be found with a detailed discussion in the appendix of Ref. [28]. $P(q,R)$ is the scattering cross section function of a rigid rod given by $P(q,R) = [2J_1(qR)/(qR)]^2$ where $J_1(x)$ denotes the Bessel function of the first kind.

The SAXS of wormlike chains in the very small q-region follow Guiner's law (i.e. $I(q) = I(0)\exp[-R_g^2q^2/3]$), which allows the determination of the radius of gyration, R_g. We determined R_g values of (5.42 ± 0.02) nm and (12.32 ± 0.05) nm for K30 and K90, respectively; the maximum q-values for curve fittings were 0.2 and 0.1 nm^{-1}.

Intensities were detected in a large q-range from 0.06 to 7.00 nm^{-1} by merging the scattering curves measured with a Kratky type camera in a capillary and from a droplet in a levitator [21,22]. The Kratky type camera produces high quality data in the region of small and the levitator setup at high q-values. Both instruments were used with synchrotron radiation as scattering source. Curve fits of the data according to Eq. (1) are shown in Fig. 1a and b for PVP K30 and K90. The best fit values for the contour length are 50 ± 1 nm and 226 ± 6 nm, which are in agreement with

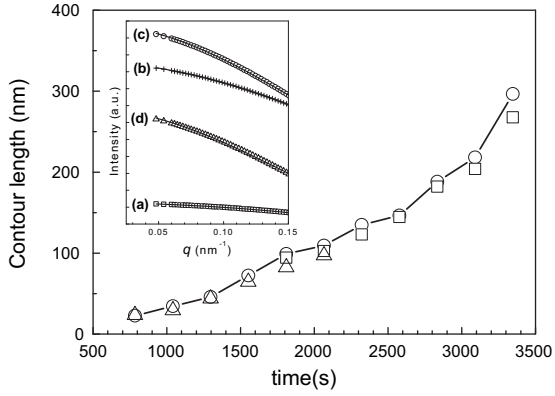

Fig. 4. The contour lengths as a function of the fraction time for PVP K30 (triangles), K90 (squares) and mixture (circles, straight line is to guide the eye). Inset: scattering curves of PVP K30 at separation times of 785 s (a), 1297 s (b), 1553 s (c) and 1809 s (d). Curve fits for determination of the contour length are given as straight lines.

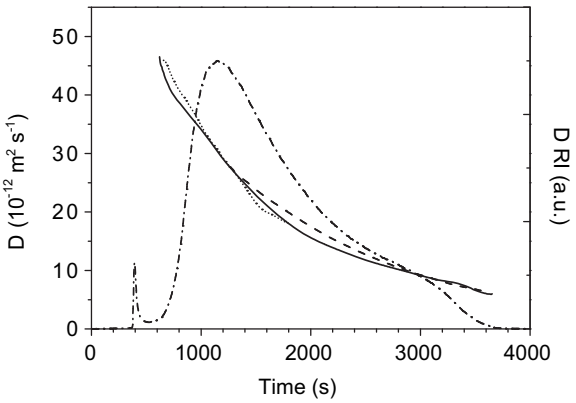

Fig. 6. Online measured diffusion coefficients as a function of the fractionation time for K30 (dotted line), K90 (dashed line) and the mixture (solid line). The RI concentration signal is given for the mixture (dashed dotted line).

the radii of gyration. The optimum Kuhn lengths for the curve fits of K30 and K90 is (3.0 ± 0.2) nm. In comparison, a MALS-SEC study of high molar mass PVP resulted in an estimated persistence length of 3 nm [14]. Pavlow et al. [13], determined $b = 2.1 \pm 0.3$ nm for PVP in 0.1 M sodium chloride solution based on viscometry and analytical ultracentrifuge measurements and the theoretical Kuhn length of atactic PVP has been calculated as $b = 1.72$ nm for a 20-mer in aqueous solution at ambient conditions [30]. Therefore, our finding for the Kuhn length is in agreement with the values reported in the literature, which were produced with other methods.

Interestingly, the scattering chain cross section is around 0.1 nm, which is identical to the backbone scattering cross section. This value is identical to the small-angle neutron scattering interpretation reported earlier by Pedersen et al. [26], for a polystyrene with deuterated backbone, i.e. where only the backbone was "visible". If we tentatively assume a compact cylinder for the PVP structure, which is clearly separated from its aqueous surroundings, the radius can be calculated between 0.4 and 0.5 nm from van der Waals' volumes. This estimated cross sectional radius is in agreement with the value reported by Pavlov et al. ($R_c = 0.50 \pm 0.13$ nm), which is an effective hydrodynamic cross section because of their study is based on hydrodynamic properties [13]. Our finding that the determined value of 0.1 nm is much lower than this leads us to the conclusion that the pyrrolidone side groups are well hydrated so that these groups do not contribute significantly to the electron density contrast. It produces obviously a contrast matching for X-rays. Conversely, the SAXS contrast for PVP is produced exclusively by the PVP backbone comparable to a deuterated backbone in SANS.

3.2. Separation with A4F

The PVP K30 and K90 were injected separately and as a binary mixture into the asymmetrical flow field-flow fractionation instrument (A4F) where an exponentially decaying crossflow profile was applied for an optimized separation (see Fig. 2, dotted line). The RI signal of the samples, which is detected first inline with SAXS and DLS, reveals that PVP K30 elutes at fractionation times from 670 to 2300 s, PVP K90 from 760 to 3500 s and the mixture from 670 to 3600 s (Fig. 2, curves a, b, and c). PVP K30 and the mixture display each a clearly visible maximum at 1030 s and 1140 s, respectively, whereas the trace of PVP K90 is without a defined maximum. It can be seen in Fig. 2 that the shapes of the traces of the two individual samples are in good agreement with the trace of the mixture. Only a slight broadening of the latter is found in comparison to the single traces which indicate a successful sample separation, as expected.

3.3. Online characterization using SAXS

The SAXS intensities were detected as the A4F separation proceeds and the radii of gyration of the fractions were determined by applying Guinier fits (not shown). The R_g values as shown in Fig. 3 range from 3.3 to 7.3 nm (PVP K30), 7.3–12.4 nm (PVP K90) and 2.9–12.9 nm (mixture). The uncertainties of the values are smaller than 0.2 nm. The increase of the R_g values with time is approximately linear with a slope of $(3.83 \pm 0.17)\ 10^{-3}$ nm s^{-1} and an intercept at (-0.05 ± 0.2) nm (straight line in Fig. 3). This finding proves that the A4F separates the PVP molecules effectively from small to large radii.

In a next step we determined the contour length by fitting the curves with the wormlike chain model according to Eq. (1) as shown in the inset of Fig. 4 exemplarily for the lower molar mass sample PVP K30 at different separation times. The curve fittings in Fig. 4 could only performed in a limited q-range (0.04–0.15 nm^{-1}) because the very low polymer concentrations after A4F separation do not allow measurement of data at higher q-values. Therefore, fixed parameter values for $b = 3.0$ nm and $R_c = 0.1$ nm were used to avoid ambiguous results. The resultant contour lengths for K30, K90 and the mixture are shown in Fig. 4. The ranges of L are 23 nm–97 nm (PVP K30), 94 nm–268 nm (PVP K90) and 23 nm–297 nm (mixture). An overview on the data is given in Table 2.

Table 1
Molar mass characteristics of PVP K30 and K90: nominal molar mass (M), contour length (L), radius of gyration (R_g) and diffusion coefficient (D). The Kuhn segment length is 3.0 ± 0.2 nm.

Polymer	M (g mol^{-1})	L (nm)	R_g (Guinier) (nm)	D (10^{-12} m^2 s^{-1})
K30	4.0×10^3	45 ± 3	5.43 ± 0.01	34.31 ± 0.51
K90	3.6×10^5	179 ± 5	12.07 ± 0.07	10.50 ± 0.26

The Benoit–Doty equation [31]

$$R_g = \left(\frac{N_k}{6} - \frac{1}{4} - \frac{1}{4N_k} - \frac{1}{8N_k^2}[1 - \exp(-2N_k)]\right)^{1/2} b \qquad (2)$$

where $N_k = L/b$ is the number of the Kuhn segment lengths allows to test the consistency of the value of the Kuhn segment length used in our work. The best curve fit of Eq. (2) to the set of the eleven R_g-L-pairs of the mixture results in $b = 3.5 \pm 0.2$ nm (see solid line in Fig. 5). The same value is found when adding the R_g-L-pairs of K30 and K90 from Table 2. In conclusion, we found that the b value from applying the Benoit–Doty equation is slightly larger than the value from the direct curve fits of the wormlike chain model (3.0 ± 0.2 nm). The small difference may result from current limitations of quality of the SAXS data.

3.4. Online determination of the diffusion coefficients

The diffusion coefficients were determined online with DLS in series directly after SAXS. It can be seen in Fig. 6 that the diffusion coefficients decrease monotonically with increasing time of fractionation for the three samples as expected. Diffusion coefficients range from 46 to 18 × 10^{-12} m^2 s^{-1} for PVP K30 and 28 to 6 × 10^{-12} m^2 s^{-1} for PVP K90. These ranges of diffusion coefficients are in agreement with the values for non-fractionated K30 and K90 (see also Table 1). The mixture of K30 and K90 covers the whole range of diffusion coefficients from 46 to 6 × 10^{-12} m^2 s^{-1} and shows a satisfactory overlay with the traces of PVP K30 and K90. The frequency distributions of the diffusion coefficients were calculated

Table 2
SAXS results for PVP K30, PVK K90 and a mixture: radii of gyration (R_g) from applying the Guinier law and contour lengths (L) from curve fits according to Eq. (1). A constant persistence length of 3.0 nm was applied. The uncertainties for R_g and L are less than 0.2 and 5 nm, respectively.

Time (s)	PVP K30		PVP K90		Mixture	
	R_g (nm)	L (nm)	R_g (nm)	L (nm)	R_g (nm)	L (nm)
784	3.3	23			2.9	23
1040	3.8	29			4.0	34
1297	4.8	44			4.8	46
1553	5.9	64			6.3	72
1809	6.7	82	7.3	94	7.4	99
2065	7.3	97	7.7	102	7.8	109
2321			8.4	123	8.8	135
2577			9.1	145	9.2	146
2834			10.3	182	10.4	188
3090			10.9	204	11.3	218
3346			12.4	268	12.9	297

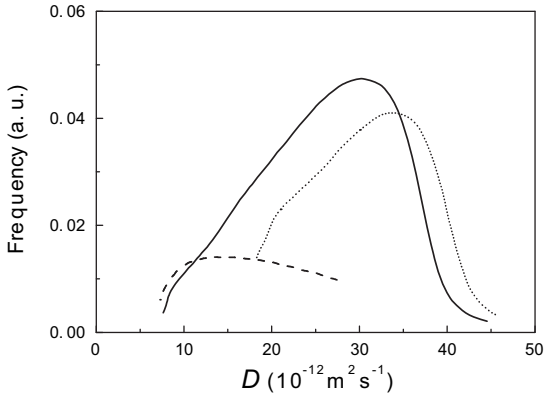

Fig. 7. Frequency of the diffusion coefficients of K30 (dotted line), K90 (dashed line) and the mixture (solid line).

by assigning the RI signal in the time interval from 623 to 3625 s to the corresponding diffusion coefficients at the same times. The results as displayed in Fig. 7 show that the frequency distribution of the mixture is correctly reproduced by the distribution of K90 at low diffusion coefficients. Similarly, the curve shape of the mixture is reproduced by the shape of the K30 at high values.

4. Conclusions

The online coupling of asymmetrical flow field-flow fractionation with small-angle scattering and dynamic light scattering has been demonstrated to be useful to characterize poly(vinyl pyrrolidone) with a broad molar mass distribution. The time required for online separation is approximately 1 h and the analysis may be performed automatically in the future. The key information are the radii of gyration and contour lengths (from SAXS) and the diffusion coefficients (from DLS). The method is versatile and can be used for a wide range of polymers with arbitrary molar mass distributions. Strong advantages are seen in comparison to the use of static light scattering for a polymer dimension smaller than 10 nm. Absolute intensity measurements [32] are planned for future investigations to assign the molar mass distributions routinely [24]. We expect a precision around 10% for the molar mass as this has already been demonstrated for proteins [33]. The attainable accuracy will probably significantly better (below 2%) in analogy to the accuracy in X-ray reflectivity [34,35].

Acknowledgment

The financial support of the Federal Institute for Materials Science and Testing is gratefully acknowledged. We thank H. Riesemeier and R. Britzke for help at the BAM*line* at BESSY. We also thank S. Rolf and F. Emmerling for experimental support in SAXS and H. Schnablegger for detailed discussions of optimized use of the SAXSess.

References

[1] Pattana-Arun J, Wolff BG. Disease of Colon and Rectum 2008;51(6):966–71.
[2] BASF Polyvinylpyrrolidone for Technical Applications. website: www.luvitec.com.
[3] Sun YG, Xia YN. Science 2002;298(5601):2176–9.
[4] Kemal L, Jiang XC, Wong K, Yu AB. Journal of Physical Chemistry C 2008;112(40):15656–64.
[5] Tadros T. Advances in Colloid and Interface Science 2009;147–148:281–99.
[6] O'Connell MJ, Boul P, Ericson LM, Huffman C, Wang YH, Haroz E, et al. Chemical Physics Letters 2001;342(3–4):265–71.
[7] Respaud M, Broto JM, Rakoto H, Fert AR, Thomas L, Barbara B, et al. Physical Review B 1998;57(5):2925–35.
[8] Ould-Ely T, Amiens C, Chaudret B, Snoeck E, Verelst M, Respaud M, et al. Chemistry of Materials 1999;11(3):526.
[9] Frank HP, Levy GB. Journal of Polymer Science 1953;10(4):371–8.
[10] Levy GB, Frank HP. Journal of Polymer Science 1955;17(84):247–54.
[11] Sneader W. Drug discovery: a history. New York: John Wiley & Sons; 2005.
[12] Ding GW, Adriane K, Chen XZ, Chen J, Liu YF. International Journal of Pharmaceutics 2007;328(1):78–85.
[13] Pavlov GM, Panarin EF, Korneeva EV, Kurochkin CV, Baikov VE, Ushakova VN. Makromolekulare Chemie-Macromolecular Chemistry and Physics 1990;191(12):2889–99.
[14] Norwood DP, Minatti E, Reed WF. Macromolecules 1998;31(9):2957–65.
[15] Minatti E, Norwood DP, Reed WF. Macromolecules 1998;31(9):2966–71.
[16] Jones SA, Martin GP, Brown MB. Journal of Pharmaceutical and Biomedical Analysis 2004;35(3):621–4.
[17] Strelitzki R, Reed WF. Journal of Applied Polymer Science 1999;73(12):2359–67.
[18] Levy GB, Caldas I, Fergus D. Analytical Chemistry 1952;24(11):1799–803.
[19] Prestel H, Niessner R, Panne U. Analytical Chemistry 2006;78(18):6664–9.
[20] Williams PS, Giddings JC. Analytical Chemistry 1987;59(17):2038–44.
[21] Leiterer J, Delissen F, Emmerling F, Thunemann AF, Panne U. Analytical and Bioanalytical Chemistry 2008;391(4):1221–8.
[22] Delissen F, Leiterer J, Bienert R, Emmerling F, Thunemann AF. Analytical and Bioanalytical Chemistry 2008;392(1–2):161–5.
[23] Glatter O. Journal of Applied Crystallography 1977;10:415–21.
[24] Glatter O, Kratky O. Small angle X-ray scattering. London: Academic Press; 1982.
[25] Fritz G, Glatter O. Journal of Physics-Condensed Matter 2006;18(36):S2403–19.
[26] Pedersen JS, Schurtenberger P. Macromolecules 1996;29(23):7602–12.
[27] Potschke D, Hickl P, Ballauff M, Astrand PO, Pedersen JS. Macromolecular Theory and Simulations 2000;9(6):345–53.
[28] Chen WR, Butler PD, Magid LJ. Langmuir 2006;22(15):6539–48.
[29] Kline SR. Journal of Applied Crystallography 2006;39:895–900.
[30] Flebbe T, Hentschke R, Hadicke E, Schade C. Macromolecular Theory and Simulations 1998;7(6):567–77.
[31] Denkinger P, Burchard W. Journal of Polymer Science Part B-Polymer Physics 1991;29(5):589–600.
[32] Orthaber D, Bergmann A, Glatter O. Journal of Applied Crystallography 2000;33:218–25.
[33] Mylonas E, Svergun DI. Journal of Applied Crystallography 2007;40:S245–9.
[34] Matyi RJ, Depero LE, Bontempi E, Colombi P, Gibaud A, Jergel M, et al. Thin Solid Films 2008;516(22):7962–6.
[35] Colombi P, Agnihotri DK, Asadchikov VE, Bontempi E, Bowen DK, Chang CH, et al. Journal of Applied Crystallography 2008;41:143–52.